ADVANCED OPTICAL MATERIALS
www.advopticalmat.de

Narrow-Band Blue-Emitting Indium Phosphide Quantum Dots Induced by Highly Active Zn Precursor

Xiaopeng Zhou, Jiejun Ren, Wenlei Cao, Andries Meijerink, and Yuhua Wang**

Colloidal indium phosphide quantum dots (In(Zn)P/ZnS QDs) show potential for application in the field of light emitting diodes (LED) and Mini/Micro-LEDs displays due to their tunable emission and low toxicity. However, the performance of blue-emitting indium phosphide QDs is still lagging behind that of red and green. Herein, a facile method to overcome this difficulty is proposed. The highly active $Zn(ClO_4)_2$ precursor is injected into the reaction mixture during the nucleation process to enhance zinc incorporation, which generates the In(Zn)P alloy QDs with enlarged bandgap. At the same time, the increase of zinc content can inhibit excessive growth of In(Zn)P QDs, and significantly improve its size distribution. The monodisperse In(Zn)P/ZnS QDs exhibit excellent blue emission (466 nm) and have the narrowest full width at half maxima (41 nm) of blue emission In(Zn)P QDs ever reported. This work provides a feasible and effective strategy for obtaining narrow-band blue-emitting In(Zn)P/ZnS QDs.

1. Introduction

In recent years, colloidal quantum dots (QDs) have drawn great attention because of the excellent optical and electronic properties induced by their unique quantum confinement.[1–8] By controlling the size and composition of colloidal particles, the electronic and optical properties of QDs can be easily tuned. The QDs possess many advantages such as continuously adjustable emission wavelength, narrow band emission, high quantum efficiency, etc., which makes QDs attractive for applications in light emitting diodes (LED, Mini/Micro-LED), displays, biomedical imaging, photoelectric detection, solar cells, and other fields.[9–19] Group II–VI semiconductor QDs (such as CdSe, CdS) have been intensively studied and have excellent performance (high luminous efficiency and narrow emission peak) with reproducible and mature synthesis method.[20–24] However, the main drawback of cadmium-containing products is their toxicity. In the European Union, the application of Cd-based materials in electrical and electronic equipment has been strictly restricted by RoHS (cadmium content cannot exceed 100 ppm).[25] As an alternative, perovskite QDs have excellent monochromatic properties and high luminescence intensity, but their intrinsic poor stability and lead toxicity still severely limit their commercial application.[26–33] Therefore, it is necessary to develop high-performance QDs materials without heavy metal elements.

In(Zn)P QDs are considered to be the most promising QDs materials for practical applications as an alternative to cadmium-based QDs due to their low toxicity properties. Group III–V InP QDs are direct bandgap semiconductors, with a bulk bandgap of 1.344 eV at room temperature.[34] Its emission can be continuously adjusted by changing the size and shell layer, from blue (≈450 nm) to near-infrared (≈750 nm).[35–37] In recent years, extensive research has been carried out on InP QDs.[38,39] Currently, the performance of green and red emitting indium phosphide QDs has been significantly improved based on the synthesis strategy with tris(trimethylsilyl)phosphine (TMSP) as phosphor precursor. By controlling the composition and thickness of the coating shell, InP/ZnSe/ZnS QDs possess a narrow full width at half maxima (FWHM) about 35 nm and ultrahigh QY nearly 100%.[40–44] Unfortunately, the TMSP is very expensive and unstable, with the risk of producing toxic gases (PH_3) when stored at under ambient conditions.[45] To solve this problem, a more environment friendly aminophosphine-based phosphor precursor has been explored, and the FWHM of the generated green- and red-emitting indium phosphide QDs could reach up to 37 nm.[46–48] However, research on blue-emitting InP QDs is still insufficient and their development is still lags far behind.

In order to obtain high performance blue-emitting InP QDs, various methods have been investigated. The most widely reported methods for the synthesis of blue-emitting InP QDs use ZnI_2 as the zinc precursor. The addition of zinc iodide (ZnI_2) in the reaction can passivate the surface of the QDs, reduce the critical size of the core, give a narrow size distribution and form In(Zn)P alloy QDs with enlarged bandgap. At the same time, the halogen ion serves as a ligand that can also inhibit the overgrowth of InP.[45,49–51] The best result for blue emitting InP QDs using ZnI_2 as the zinc precursor is reported

X. Zhou, J. Ren, W. Cao, A. Meijerink, Y. Wang
School of Materials and Energy
National and Local Joint Engineering Laboratory for Optical Conversion Materials and Technology of National Development and Reform Commission Lanzhou University
Lanzhou 730000, P. R. China
E-mail: wyh@lzu.edu.cn
A. Meijerink
Debye Institute for Nanomaterials Science
Utrecht University
Utrecht 3584CC, The Netherlands
E-mail: a.meijerink@uu.nl
The ORCID identification number(s) for the author(s) of this article can be found under https://doi.org/10.1002/adom.202202128.

DOI: 10.1002/adom.202202128

by Sun's group, which exhibit narrow FWHM of 45 nm.[52] In recent years, Ga^{3+} doping is considered to be a potential way to obtain high performance blue emitting InP QDs. The bandgap of GaP is larger than that of InP, and the bandgap of In(Ga)P QDs increases with Ga doping.[53,54] For example, Yang et al. successfully prepared blue emitting In(Ga)P/ZnS QDs with an emission wavelength of 465 nm by means of In^{3+}-to-Ga^{3+} cation exchange reaction, but the emission band is broad.[55] Lee's group synthesized blue emitting In(Ga)P/ZnS QDs with a FWHM of 46 nm by the method of heating Ga, In, and P precursors together.[56] However, the FWHMs of the blue emitting InP QDs obtained by these strategies are still too large compared to the red and green emitting InP QDs.

In this work, we discuss the influence of zinc precursors on the properties of QDs, and propose a new strategy for preparing narrow-band blue-emission In(Zn)P/ZnS QDs by using highly reactive $Zn(ClO_4)_2$ as zinc precursor. The environmental friendly $(DMA)_3P$ was used as the phosphine precursor and ZnI_2 was used as the zinc precursor to prepare In(Zn)P QDs. During the nucleation process, $Zn(ClO_4)_2$ was injected to control the emission wavelength of the InP QDs. Different from ZnI_2, the highly active $Zn(ClO_4)_2$ will produce more active zinc ions for the reaction, forming an In(Zn)P alloy with an enlarged bandgap, which is manifested by a blueshift in emission and absorption spectra. Theoretical calculations also verify that the entry of Zn^{2+} into the InP lattice increases the bandgap of InP. At the same time, the Zn precursor can stabilize the surface of the In(Zn)P QDs and ultimately narrow its size distribution. The prepared In(Zn)P/ZnS QDs exhibit excellent monochromaticity, with an emission wavelength of 466 nm and a FWHM of 41 nm.

2. Results and Discussion

In this work, indium phosphide QDs were prepared by injecting $(DMA)_3P$ into the indium halide precursor dissolved in oleylamine (OAm) at high temperature, and the effect of zinc precursor on the properties of In(Zn)P QDs was investigated. The growth of In(Zn)P QDs was monitored by UV–vis absorption spectroscopy and transmission electron microscopy (TEM) images (**Figure 1**). The absorption peak exhibited a blueshift from 520 to 430 nm when replacing $ZnCl_2$ with ZnI_2, accompanied by a decrease in the average size of the QDs. Analysis of TEM images shows that the average diameter of In(Zn)P QDs decreased from 3.1 to 2.7 nm. After coating the ZnS shell to passivate In(Zn)P surface defects, the emission of In(Zn)P/ZnS QDs showed a shift from red (for In(Zn)P/ZnS made with a $ZnCl_2$ precursor) to green (for a ZnI_2 precursor, see Figure S1a,b, Supporting Information). The blueshift of the emission peak is attributed directly to the fact that ZnI_2 has a lower stability than $ZnCl_2$ and using the more reactive ZnI_2 to replace $ZnCl_2$ can speed up reaction rate and effectively inhibit the growth of QDs, excess Zn^{2+} also can effectively passivate the surface of InP QDs and activate phosphorus precursors, inhibit the growth of QDs in the form of Oswald ripening, resulting in smaller In(Zn)P QDs with a more uniform particle size distribution.[45,50–52]

Unfortunately, the higher reactive ZnI_2 precursor seems to be still insufficient to form blue-emitting In(Zn)P QDs and suppress growth of QDs to obtain blue-emitting QDs. The QDs also show rather broad emission spectra with a FWHM larger than 45 nm (Figure S1c, Supporting Information). Therefore, we tried to use zinc perchlorate [$Zn(ClO_4)_2$)] with higher activity than ZnI_2 to optimize the emission wavelength and size distribution of blue-emitting In(Zn)P QDs. The synthesis process is shown in **Scheme 1**. $Zn(ClO_4)_2$ was injected as a highly reactive zinc precursor to prepare smaller In(Zn)P QDs. Figure 1e shows the absorption spectrum and it can be clearly observed that the absorption peak was further blueshifted after $Zn(ClO_4)_2$ injection. Figure S2 (Supporting Information) shows the absorption spectra of In(Zn)P QDs prepared with different amounts of $Zn(ClO_4)_2$. With the gradual increase of injected $Zn(ClO_4)_2$, the absorption spectra blueshifted from 414 to 394 nm, accompanied by a narrowing of the absorption peak. The narrowing reflects the improvement of the size distribution of QDs, indicating that $Zn(ClO_4)_2$ can effectively inhibit the further growth of QDs. Figure 1f shows that the QDs have a uniform size distribution, with an average size of 2.63 nm. High-resolution TEM shows the high crystallinity In(Zn)P QDs with a crystal interplanar spacing of 0.206 nm, which is in agreement with the (220) crystal plane of cubic InP (Figure S3, Supporting Information).

In addition to the decrease of size, the increase of Zn content in In(Zn)P QDs can also explain the observed increase of the bandgap,[50,57,58] which is reflected by the blueshift of the absorption peak. The X-ray diffraction (XRD) pattern of the sample synthesized without Zn^{2+} precursor is shown in **Figure 2**a and corresponds to the cubic zinc blende structure of InP [JCPDF: 32-0452]. When the Zn precursor was added to the reaction, the sample showed the same diffraction pattern as InP, and no diffraction peaks of by-products appeared. However, the diffraction peaks shift toward larger angles (Figure 2a), which indicates a contraction of InP crystal lattice which is expected upon forming In(Zn)P alloy QDs in view of the smaller ionic radius of Zn^{2+} compared to In^{3+}. The shift of the diffraction peak confirms the Zn^{2+} alloying in In(Zn)P QDs rather than Zn^{2+} being located on the surface of QDs, because Zn^{2+} in a surface layer could not lead to the shift of the InP core XRD peaks. And with the addition of $Zn(ClO_4)_2$, the diffraction peak further shifts to a large angle, indicating that the doping of Zn was enhanced.

Inductively coupled plasma (ICP) analysis confirmed that the addition of $Zn(ClO_4)_2$ increased the Zn^{2+} content in In(Zn)P (**Table 1**). The In/Zn ratio of In(Zn)P QDs obtained with ZnI_2 as a precursor was 1:0.88, but the In/Zn ratio increased to 1:1.33 when 0.55 mmol $Zn(ClO_4)_2$ was injected. The presence of Zn^{2+} in the sample can also be detected in the EDX energy spectrum (Figure S4, Supporting Information). The results showed that the In/Zn ratio had the same increasing trend as found with ICP analysis after the addition of $Zn(ClO_4)_2$ (Table S1, Supporting Information), which proved that the addition of Zn^{2+} contributes to the blueshift of the absorption spectrum.

We further investigated the chemical composition of InP by X-ray photoelectron spectroscopy (XPS). It was confirmed that In(Zn)P alloy QDs formed and the Zn content increased after $Zn(ClO_4)_2$ injection. The signals of In, P, and Zn could be clearly observed in the XPS spectra of In(Zn)P QDs (Figure 2b). The pure phase InP QD sample shows the In $3d_{5/2}$ and In $3d_{3/2}$ peak centered at 444.1 and 452 eV, a typical value for In^{3+}

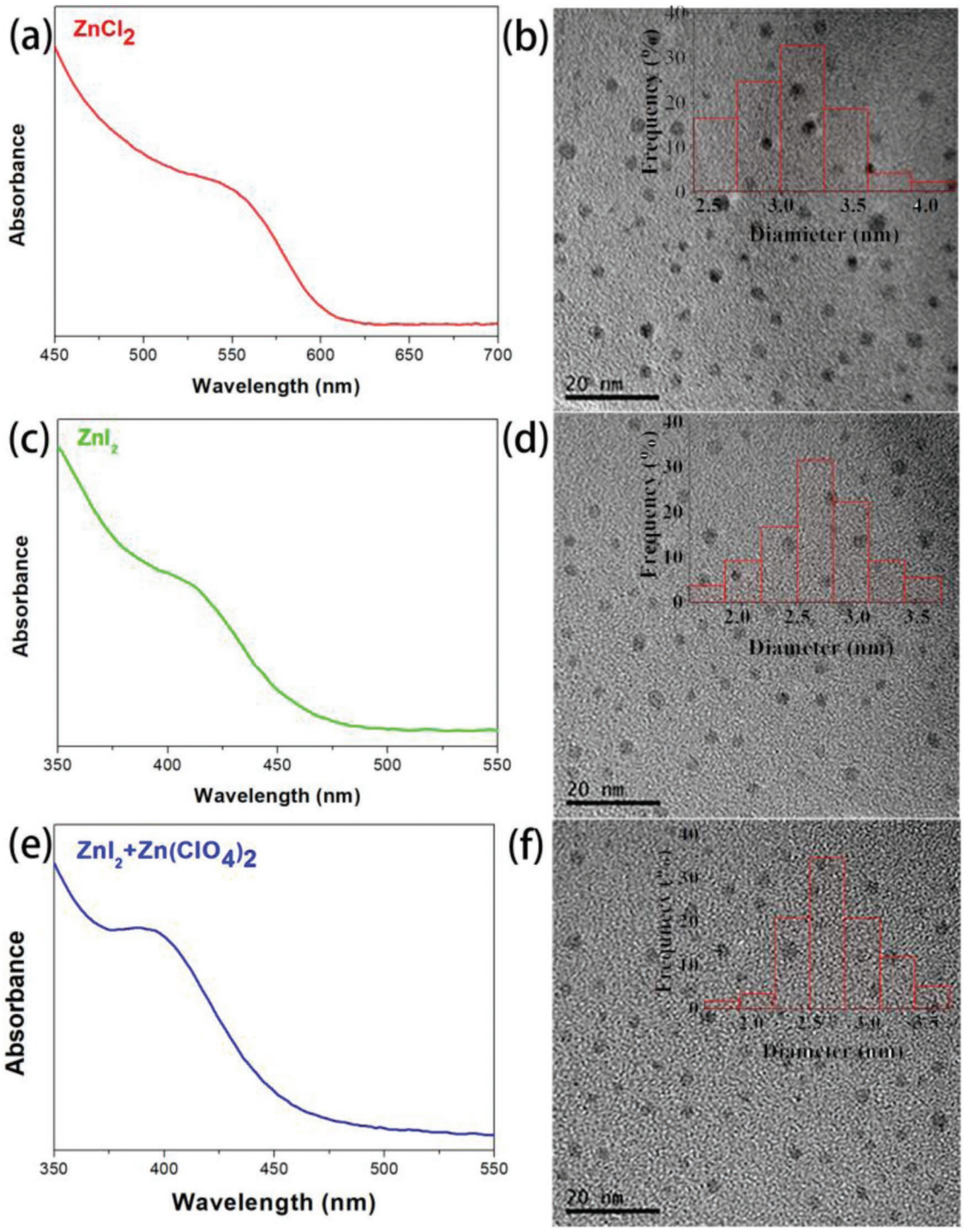

Figure 1. Absorption spectra and TEM images of In(Zn)P QDs prepared by a,b) $ZnCl_2$, c,d) ZnI_2, and e,f) ZnI_2+$Zn(ClO_4)_2$.

compounds.[59,60] After adding ZnI_2 during the synthesis, a systematically shifting of both the In $3d_{5/2}$ and In $3d_{3/2}$ peaks to higher binding energies is observed (Figure 2c). The peaks of In $3d_{5/2}$ and In $3d_{3/2}$ shifted to 444.8 and 452.35 eV, respectively. At the same time, the Zn $3d_{3/2}$ peak at 1021.1 eV can be observed (Figure 2d). The shift of In 3d peaks and the appearance of Zn $3d_{3/2}$ peak is explained as a result of the altered chemical environment of In^{3+} and the formation of the In(Zn)P alloy QD. The In signals and Zn signals further shift toward higher binding energy with the injection of $Zn(ClO_4)_2$, which indicates an increase of Zn content in In(Zn)P.

I^- and oleylamine (N) are considered as ligands, and the signal can also be clearly observed in the XPS spectra (Figure 2b). However, no Cl signal was detected, and no Cl peak appeared even in the high-resolution XPS spectra (Figure 2e,f). It is evident that ClO^{4-} does not act as a ligand to inhibit the

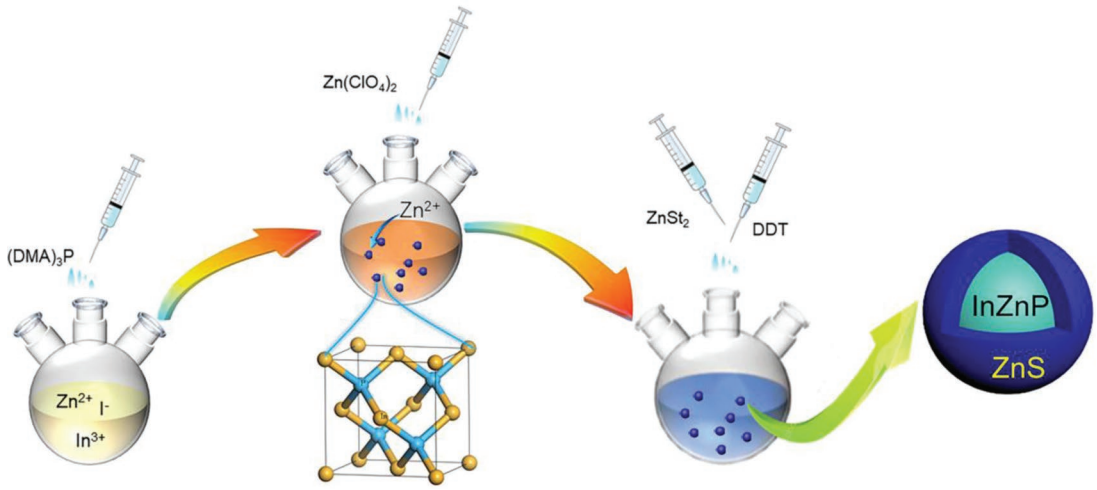

Scheme 1. Schematic illustration for the synthesis of blue-emission In(Zn)P/ZnS QDs.

overgrowth of In(Zn)P QDs as I^- does. In combination with the data of XRD and ICP analysis, the blueshift of In(Zn)P QDs absorption caused by the addition of $Zn(ClO_4)_2$ was interpreted as the result of the increase of Zn^{2+} concentration giving rise to smaller QDs with a higher Zn^{2+} content. The calculated band structures of InP and InZnP suggest that the addition of Zn^{2+} to InP leads to an increase of bandgap (Figure S5, Supporting Information). This result is consistent with the increase in the Zn^{2+} content leading to the blueshift of the absorption and the increase in the bandgap and also provide theoretical support for the experimental results.

Due to the large number of defects on the surface of QDs, nonradiative relaxation lead to the decrease of QY (generally less than 1%) for core-only QDs. Generally, ZnSe and ZnS with zinc blende structure are epitaxially grown on the surface of In(Zn)P QDs as shell materials to passivate the surface defects. The bandgaps of InP, ZnSe, and ZnS are 1.35, 2.70, and 3.68 eV, respectively. Electrons will delocalize into the shell when ZnSe with a smaller bandgap (compared to ZnS) was used as the shell material, which leads to the reduction of the bandgap (less confinement) and the redshift of emission peak.[48,61] ZnS with a larger bandgap reduces the delocalization of electrons, which

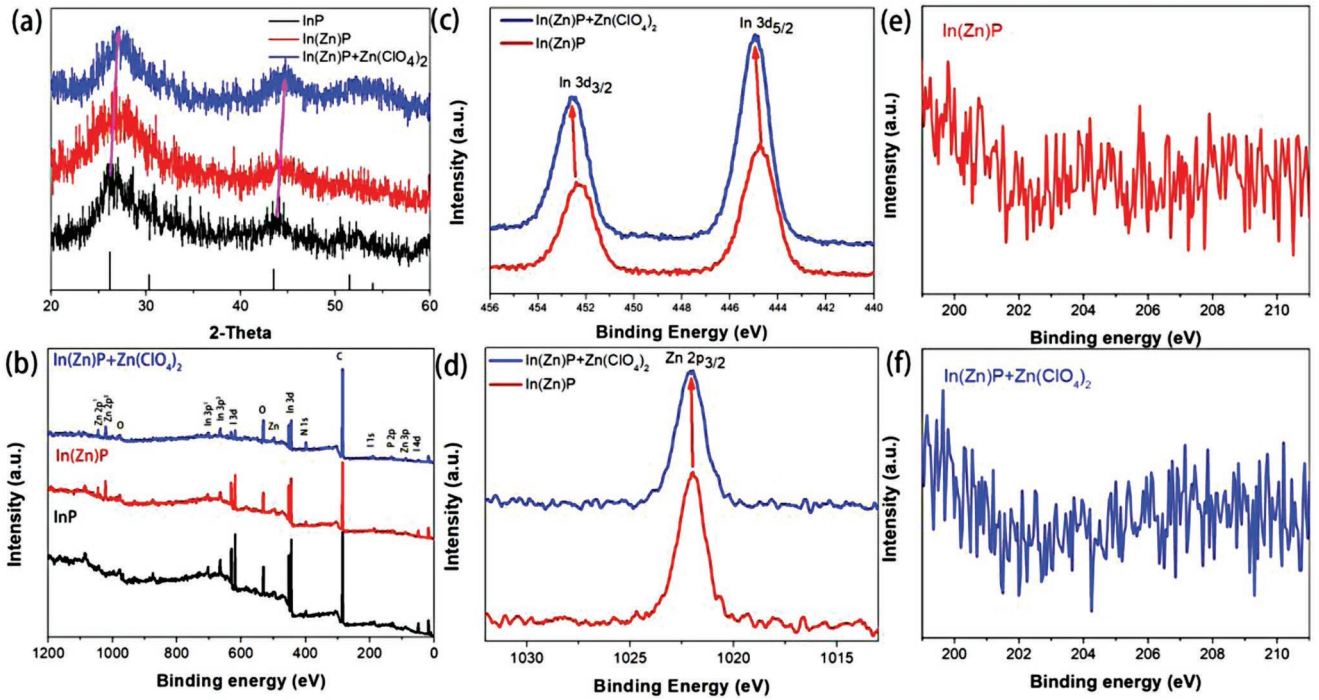

Figure 2. a) XRD diffraction patterns and b) XPS energy spectra of InP QDs and the In(Zn)P QDs obtained by $Zn(ClO_4)_2$ injection. High-resolution XPS spectra of c) In 3d, d) Zn 2p, and e,f) Cl for In(Zn)P QDs.

Table 1. Ions content in In(Zn)P samples as determined by ICP-AES.

	In	Zn	In/Zn [mol]
In(Zn)P	4.671 mg L^{-1}	2.350 mg L^{-1}	1: 0.88
In(Zn)P+Zn$(ClO_4)_2$	3.165 mg L^{-1}	2.394 mg L^{-1}	1: 1.33

is conducive to obtain blue-emitting In(Zn)P QDs (Figure S6, Supporting Information).

Not only the cation precursor affects the optical properties of indium phosphide QDs, also the sulfur precursor can be varied. Two sulfur precursors, TOP-S and 1-dodecanethiol (DDT), were used to grow the ZnS shell. The indium phosphide QDs synthesized by TOP-S have longer emission wavelength than those synthesized by DDT, and exhibit broader absorption and emission peaks (**Figure 3**b). Due to the lower reactivity of TOP-S, the coating of the ZnS shell proceeded slowly, which leads to the further growth of In(Zn)P at high temperature. This process also may involve Oswald ripening and finally leads to a shift of the emission spectrum in the direction of longer wavelengths and a simultaneous broadening of the emission spectrum. The higher reactivity of DDT enabled the rapid growth of ZnS shell and inhibited the growth of In(Zn)P, resulting in In(Zn)P/ZnS QDs with shorter emission wavelength and narrower FWHM. After coating with the ZnS shell, the diffraction peaks of In(Zn)P QDs shift to larger angles, which are closer to the diffraction peaks of ZnS (JCPDS No. 99-0097), as shown in Figure 3a. However, larger size nanoparticles could be found in the TEM image after encapsulating the ZnS shell (Figure 3c) while no impurity phase was detected in the XRD pattern. Some larger nanoparticles were identified as zinc stearate microspheres, which were produced by the excess zinc stearate in the reaction.[52] By continuing adding sulfur precursors to the reaction mixture and extending the reaction time, zinc stearate microspheres could be easily removed, and the reaction of reinjected the sulfur precursor did not cause a further shift of the emission peak or broadening of the FWHM (Figure S7, Supporting Information). The TEM image is consistent with the XRD results (Figure 3d), showing a larger average size of In(Zn)P/ZnS QDs (4.8 nm) compared to the In(Zn)P core (2.6 nm). This result clearly indicates that ZnS shell has been epitaxially grown on the InP core with the thickness about 2 nm. High-resolution TEM shows a clear interplanar spacing of 0.312 nm, which is in good agreement with the distance between (111) crystal planes of cubic ZnS (Figure S8, Supporting Information).

The blue-emitting indium phosphide QDs were prepared by coating ZnS shell with DDT as a sulfur precursor to passivate the surface. It was observed that with a gradual increase of $Zn(ClO_4)_2$ addition the absorption peak of In(Zn)P/ZnS QDs blueshifted and narrowed (Figure S9, Supporting Information), which is in agreement with the change of In(Zn)P QDs (smaller size, more uniform and increased Zn content). The same trends can also be observed in the emission spectra, as shown in **Figure 4**a. The emission wavelength blueshifted from 478 to 463 nm (Figure 4b) while the FWHM of In(Zn)P/ZnS QDs reduced from 49 to 41 nm with the addition of $Zn(ClO_4)_2$,

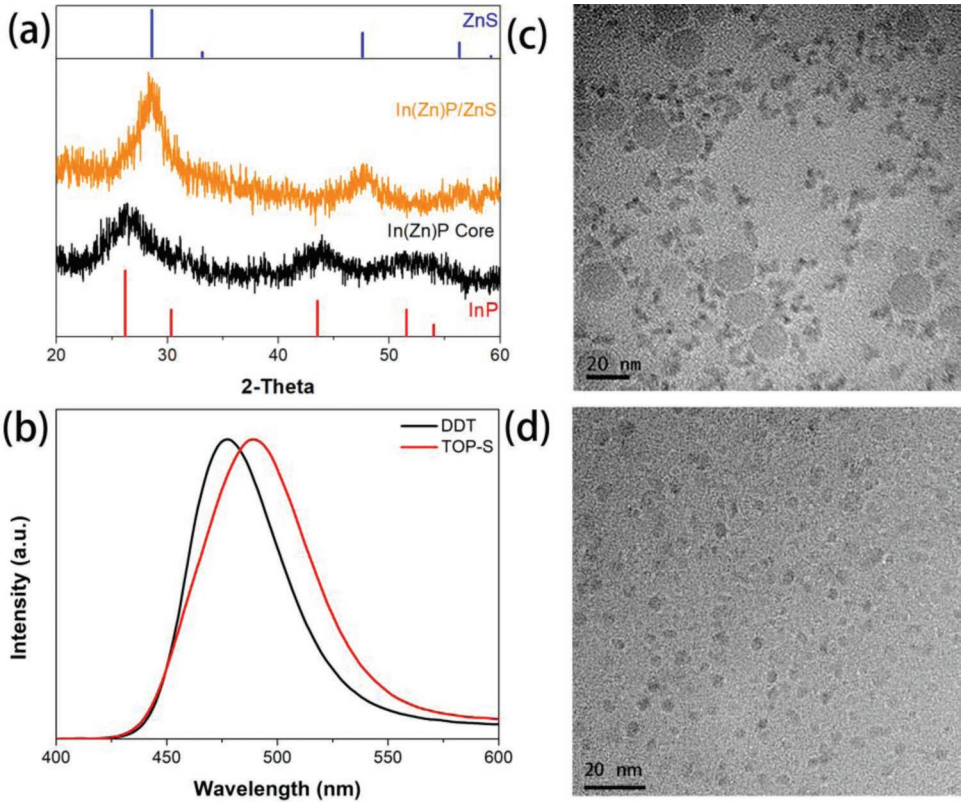

Figure 3. a) XRD patterns of In(Zn)P and In(Zn)P/ZnS QDs. b) Emission spectra of In(Zn)P/ZnS QDs obtained by using TOP-S and DDT, respectively. c,d) TEM images of products after coating ZnS with different amount of TOP-S (4.6 and 6.3 mmol).

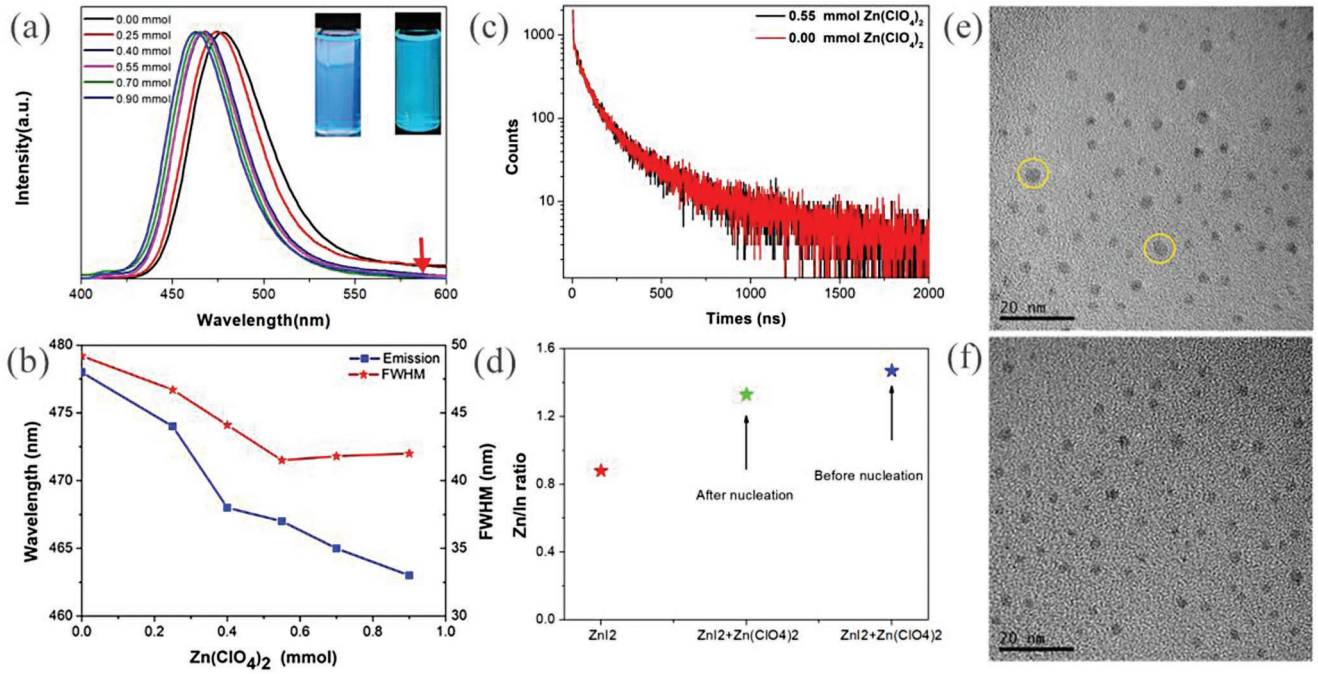

Figure 4. a) Emission spectra, b) emission maximum and FWHM, and c) time-resolved PL decays of In(Zn)P/ZnS QDs obtained by varying $Zn(ClO_4)_2$ amounts. d) ICP-AES-based Zn/In ratio of In(Zn)P/ZnS QDs obtained by using different addition methods of $Zn(ClO_4)_2$. e) TEM image of In(Zn)P QDs obtained without $Zn(ClO_4)_2$ injection. f) TEM image of In(Zn)P QDs obtained with $Zn(ClO_4)_2$ injection.

which is consistent with the uniform size distribution of In(Zn)P QDs. Comparing the TEM images of In(Zn)P QDs before and after the addition of $Zn(ClO_4)_2$, it was found that the large size In(Zn)P nanoparticles disappeared after the addition of $Zn(ClO_4)_2$ (Figure 4e,f). The emission spectra of In(Zn)P/ZnS QDs show that at the same time the long-wavelength tail disappeared (Figure 4a). The obtained In(Zn)P/ZnS QDs had good luminescence properties with the photoluminescence quantum yield (PLQY) of 34% (Figure S10, Supporting Information), slightly higher than for the sample without adding $Zn(ClO_4)_2$ which shows a PLQY of 31%. This result indicates that the addition of $Zn(ClO_4)_2$ has no strong effect on the PLQY of the QDs. Furthermore, the time-resolved PL decays of In(Zn)P/ZnS QDs confirmed that the addition of $Zn(ClO_4)_2$ did not introduce additional defects (Figure 4c). The time-resolved PL decay curves of two samples are nearly identical and can be fitted by the three-exponential function. The average lifetimes (τ_{ave}) of two samples were calculated as 173 and 164 ns, respectively.

To further investigate the role of the reactivity of the Zn precursor we also tried to partially replace ZnI_2 with $Zn(ClO_4)_2$ during the nucleation process while keeping the amount of Zn unchanged, instead of adding $Zn(ClO_4)_2$ after injecting P precursor. The emission spectra of In(Zn)P/ZnS QDs showed a significant blueshift from 480 to 443 nm after the addition of $Zn(ClO_4)_2$ (Figure S11, Supporting Information). The blueshift is ascribed to the fact that highly active $Zn(ClO_4)_2$ can be easily dissociated to form Zn^{2+} entering the InP lattice and leading to an increase of the bandgap and the suppress of the growth of In(Zn)P QDs. ICP analysis and TEM confirmed the increase of zinc content in In(Zn)P QDs (Figure 4d) and decrease in particle size (Figure S12, Supporting Information). However, the addition of highly active precursor at the early stage of nucleation leads to higher reaction rates, resulting in poorer size distribution, which is manifested by a significant broadening of the emission spectra (Figure S11, Supporting Information). Therefore, we injected $Zn(ClO_4)_2$ into the reaction after the P precursor was added to reduce the influence of $Zn(ClO_4)_2$ on nucleation while using the Zn^{2+} to regulate the bandgap of In(Zn)P QDs. By changing the time of injection, we found that when $Zn(ClO_4)_2$ was injected 3 min after the start of nucleation, the FWHM of In(Zn)P/ZnS QDs shows the optimal values (Figure S13, Supporting Information).

As mentioned in the Experimental Section, the injected $Zn(ClO_4)_2$ precursor was $Zn(ClO_4)_2 \cdot 6H_2O$. In addition to Zn^{2+} which affects the nucleation of QDs, water molecules have also been proposed to have an effect on the size and emission of QDs.[62,63] Although $Zn(ClO_4)_2 \cdot 6H_2O$ was dissolved in OAm and degassed at 140 °C for 1 h to remove water molecules before injection, it is important to rule out that residual water molecules in $Zn(ClO_4)_2 \cdot 6H_2O$ affected the performance of QDs. The In(Zn)P QDs were prepared by injecting 0.55 mmol ZnI_2 or 0.55 mmol ZnI_2+3.3mmol H_2O (using the same pretreatment as $Zn(ClO_4)_2 \cdot 6H_2O$). The emission spectra are shown in Figure S14 (Supporting Information). After the injection of ZnI_2 or ZnI_2+H_2O, the emission spectra of the resulting QDs slightly blueshift about 6 nm. There is no obvious effect of water molecules on the In(Zn)P/ZnS QDs, which means that the water molecules were completely removed during the degassing process. This confirms that the shift of the emission peak to the short wavelength direction was induced by the increase of Zn^{2+}. Compared with ZnI_2, the addition of $Zn(ClO_4)_2 \cdot 6H_2O$ results in a larger blueshift, which indicates

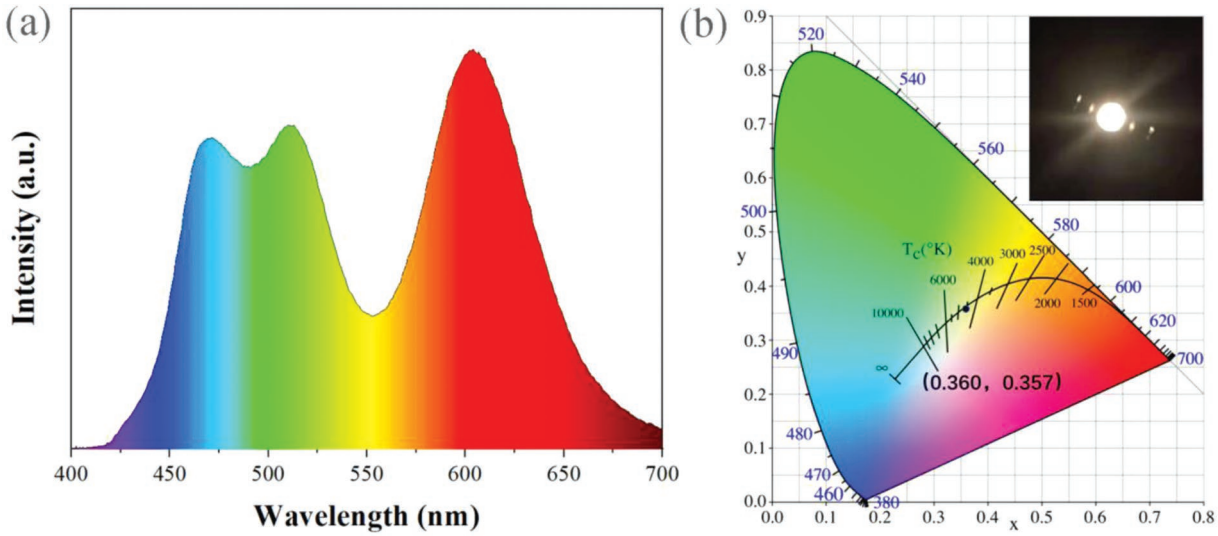

Figure 5. a) Emission spectrum and b) CIE color coordinates of the LED (50 mA). Inset: Photograph of the indium phosphide QDs LED.

that the $Zn(ClO_4)_2$ is more active than ZnI_2 and can dissociate more rapidly to form Zn^{2+}.

To further explore the potential application in LED, LED devices were fabricated by using a UV chip to excite the In(Zn)P/ZnS QDs. By modifying the ratio of the blue, green, and red In(Zn)P/ZnS, a white In(Zn)P/ZnS LED could be obtained, the emission spectrum is shown in **Figure 5**a. The obtained LEDs showed good luminous performance (Figure 5b) with a high color rendering index value of 78.4 and a low correlated color temperature of 4497 K. The CIE coordinates of the white LED are (0.360, 0.357), indicating a white emission.

3. Conclusions

In summary, in this work, we demonstrated an effective method to enable the formation of narrow-band blue-emitting indium phosphide QDs by adding the highly reactive $Zn(ClO_4)_2$ precursor. It was shown that $Zn(ClO_4)_2$ enhances the incorporation of Zn^{2+} into InP and leads to larger bandgap In(Zn)P alloy QDs. After coating with the larger bandgap ZnS shell to effectively suppress the delocalization of electrons from InP core to shell, we obtained narrow band blue-emitting indium phosphide QDs with the emission peak at 466 nm. Zn^{2+} can also inhibit further growth of In(Zn)P QDs, resulting in a more uniform size distribution of In(Zn)P QDs. Correspondingly, the FWHM of In(Zn)P/ZnS QDs significantly narrowed from 49 to 41 nm, which is the narrowest FWHM for blue-emitting InP QDs ever reported. This work not only explored the influence of zinc precursor on the optical properties and performance of InP QDs, but also provided a new strategy for the size-focused growth of In(Zn)P/ZnS QDs.

4. Experimental Section

Chemicals: Indium chloride ($InCl_3$, 99.99%, Aladdin), zinc iodide (ZnI_2, 99.99%, Aladdin), zinc stearate ($ZnSt_2$, 10%–12% Zn basis, Aladdin), zinc perchlorate hexahydrate ($Zn(ClO_4)_2.6H_2O$ 99.9%, Aladdin), OAm (90%, Aladdin), 1-octadecene (ODE, 90%, Aladdin), tris(dimethylamino)phosphine ($P(N(CH_3)_2)_3$, $(DMA)_3$ P,98%, Aladdin), DDT (98%), and trioctylphosphine (TOP, 90%, Aladdin) were used without any further purification.

Synthesis of $Zn(ClO_4)_2$ Precursor: 205 mg $Zn(ClO_4)_2{\cdot}6H_2O$ was mixed with 2 mL OAm in a three-necked flask and degassed at 140 °C for 1 h to produce $Zn(ClO_4)_2$ precursor.

Synthesis of TOP-S(2M): 640 mg sulfur was added to 10 mL TOP at room temperature and stirred until the sulfur was completely dissolved.

Synthesis of In(Zn)P QDs: 100 mg $InCl_3$, 702 mg ZnI_2, and 5 mL OAm were placed in a three-necked flask. To completely dissolve $InCl_3$, ZnI_2 powders and remove water, the mixture was degassed for 1 h at 130 °C. After that, the mixture was heated to 200 °C under N_2 flow. Then, 2.48 mmol $P(N(CH_3)_2)_3$ was injected into the mixture and kept at 200 °C for 20 min. The crude In(Zn)P solution was precipitated in ethanol and collected centrifugation at 16 000 rpm for 3 min. The products were dispersed in hexane.

Synthesis of In(Zn)P QDs by $Zn(ClO_4)_2$ Treatment: Similar to the previously described synthesis method, but now the $Zn(ClO_4)_2$ precursor was introduced after the injection of the phosphorus precursor. 3 min after nucleation, 2 mL of $Zn(ClO_4)_2$ precursor was injected and kept at 200 °C for 20 min. The crude In(Zn)P solution was precipitated in ethanol and collected centrifugation at 16 000 rpm for 3 min. The products were dispersed in hexane.

Synthesis of Core–Shell Structured In(Zn)P/ZnS QDs: After the synthesis of In(Zn)P core, instead of cooling to room temperature, 6.3 mmol DDT and 2.4 mmol $ZnSt_2$ mixed with 19 mmol ODE were injected into the crude In(Zn)P solution. The reaction was then ramped up to 300 °C, and held at that temperature for 45 min. The purification process of In(Zn)P/ZnS QDs is the same as for In(Zn)P QDs.

Fabrication of White LED: A white LED was manufactured by using a UV LED chip (λ_{max} = 365 nm) to excite red-, green-, and blue-emitting InP/ZnS QDs. In(Zn)P/ZnS QDs were dispersed in the ultraviolet (UV) curing adhesive and combined with the chip, the mixture was solidified under UV light.

Characterization: The XRD of products was observed using a Bruker D2 phaser X-ray diffractometer (Cu Kα, λ = 1.54056 Å, 30 kV, 15 mA). The morphology and size of the nanocrystals were characterized by TEM operating at 300 kV (Tecnai G2 F30). The elemental analysis was investigated by inductively coupled plasma optical emission spectroscopy (ICP-OES, Plasma Quant PQ9000). The XPS spectra were recorded by a Kratos AXIS Ultra DLD spectrometer. PL spectra were investigated using Fluorolog-3 spectrophotometer (Horiba Jobin Yvon).

The QYs were determined using an Edinburgh Instruments FLS920 spectrophotometer. UV–vis absorption spectra were recorded by a PerkinElmer Lambda 950 spectrometer.

Supporting Information

Supporting Information is available from the Wiley Online Library or from the author.

Acknowledgements

The authors gratefully acknowledge the financial support from the National Natural Science Foundation of China (No. U1905213).

Conflict of Interest

The authors declare no conflict of interest.

Data Availability Statement

The data that support the findings of this study are available from the corresponding author upon reasonable request.

Keywords

blue emission, indium phosphide, quantum dots, size focusing, zinc perchlorate

Received: September 11, 2022
Revised: December 14, 2022
Published online: January 9, 2023

[1] Y. M. Sung, T. G. Kim, D. J. Yun, M. Lim, D. S. Ko, C. Jung, N. Won, S. Park, W. S. Jeon, H. S. Lee, J. H. Kim, S. Jun, S. Sul, S. Hwang, *Small* **2021**, *17*, 2102792.
[2] J. Kim, H. S. Choi, A. Wedel, S.-Y. Yoon, J.-H. Jo, H.-M. Kim, C.-J. Han, H.-J. Song, J.-M. Yi, J.-S. Jang, H. Zschiesche, B.-J. Lee, K. Park, H. Yang, *J. Mater. Chem. C* **2021**, *9*, 4330.
[3] L. Angele, S. Dreyfuss, B. Dubertret, N. Mezailles, *Inorg. Chem.* **2021**, *60*, 2271.
[4] I. Lignos, Y. Mo, L. Carayannopoulos, M. Ginterseder, M. G. Bawendi, K. F. Jensen, *React. Chem. Eng.* **2021**, *6*, 459.
[5] R. Toufanian, M. Chern, V. H. Kong, A. M. Dennis, *Chem. Mater.* **2021**, *33*, 1964.
[6] R. Valleix, Q. Zhang, D. Boyer, P. Boutinaud, G. Chadeyron, Y. Feng, H. Okuno, F. Reveret, H. Hintze-Bruening, F. Leroux, *Adv. Mater.* **2021**, *33*, 2103411.
[7] H. Shen, Q. Gao, Y. Zhang, Y. Lin, Q. Lin, Z. Li, L. Chen, Z. Zeng, X. Li, Y. Jia, S. Wang, Z. Du, L. S. Li, Z. Zhang, *Nat. Photonics* **2019**, *13*, 192.
[8] C. Xia, W. Wu, T. Yu, X. Xie, C. van Oversteeg, H. C. Gerritsen, C. de Mello Donega, *ACS Nano* **2018**, *12*, 8350.
[9] C. Li, C. Han, Y. Zhang, Z. Zang, M. Wang, X. Tang, J. Du, *Sol. Energy Mater. Sol. Cells* **2017**, *172*, 341.
[10] F. McGrath, U. Ghopade, K. M. Ryan, *J. Chem. Phys.* **2020**, *152*, 174702.
[11] J. Zhou, Y. Yang, C. Y. Zhang, *Chem. Rev.* **2015**, *115*, 11669.
[12] H. Moon, C. Lee, W. Lee, J. Kim, H. Chae, *Adv. Mater.* **2019**, *31*, 1804294.
[13] C. Zhou, J. M. Pina, T. Zhu, D. H. Parmar, H. Chang, J. Yu, F. Yuan, G. Bappi, Y. Hou, X. Zheng, J. Abed, H. Chen, J. Zhang, Y. Gao, B. Chen, Y.-K. Wang, H. Chen, T. Zhang, S. Hoogland, M. I. Saidaminov, L. Sun, O. M. Bakr, H. Dong, L. Zhang, E. H. Sargent, *Adv. Sci.* **2021**, *8*, 2101125.
[14] M. Shalom, Z. Tachan, Y. Bouhadana, H.-N. Barad, A. Zaban, *J. Phys. Chem. Lett.* **2011**, *2*, 1998.
[15] E. Jang, Y. Kim, Y.-H. Won, H. Jang, S.-M. Choi, *ACS Energy Lett.* **2020**, *5*, 1316.
[16] Y. Weng, S. Chen, Y. Zhang, L. Sun, Y. Wu, Q. Yan, T. Guo, X. Zhou, C. Wu, *Opt. Laser Technol.* **2021**, *140*, 107026.
[17] A. M. Saeboe, A. Y. Nikiforov, R. Toufanian, J. C. Kays, M. Chern, J. P. Casas, K. Han, A. Piryatinski, D. Jones, A. M. Dennis, *Nano Lett.* **2021**, *21*, 3271.
[18] Y. Chen, P. Kivisaari, M. E. Pistol, N. Anttu, *Nanotechnology* **2018**, *29*, 045401.
[19] M. Gao, H. Yang, H. Shen, Z. Zeng, F. Fan, B. Tang, J. Min, Y. Zhang, Q. Hua, L. S. Li, B. Ji, Z. Du, *Nano Lett.* **2021**, *21*, 7252.
[20] A. Ashokan, P. Mulvaney, *Chem. Mater.* **2021**, *33*, 1353.
[21] F. S. Riehle, K. Yu, *Chem. Mater.* **2020**, *32*, 1430.
[22] O. Chen, J. Zhao, V. P. Chauhan, J. Cui, C. Wong, D. K. Harris, H. Wei, H. S. Han, D. Fukumura, R. K. Jain, M. G. Bawendi, *Nat. Mater.* **2013**, *12*, 445.
[23] T. VanWie, E. Wysocki, J. R. McBride, S. J. Rosenthal, *Chem. Mater.* **2019**, *31*, 8558.
[24] T. Zhao, E. D. Goodwin, J. Guo, H. Wang, B. T. Diroll, C. B. Murray, C. R. Kagan, *ACS Nano* **2016**, *10*, 9267.
[25] S. Tamang, C. Lincheneau, Y. Hermans, S. Jeong, P. Reiss, *Chem. Mater.* **2016**, *28*, 2491.
[26] J. Ren, X. Dong, G. Zhang, T. Li, Y. Wang, *New J. Chem.* **2017**, *41*, 13961.
[27] Y. H. Song, J. S. Yoo, B. K. Kang, S. H. Choi, E. K. Ji, H. S. Jung, D. H. Yoon, *Nanoscale* **2016**, *8*, 19523.
[28] J. Ren, T. Li, X. Zhou, X. Dong, A. V. Shorokhov, M. B. Semenov, V. D. Krevchik, Y. Wang, *Chem. Eng. J.* **2019**, *358*, 30.
[29] J. Ren, X. Zhou, Y. Wang, *Chem. Eng. J.* **2020**, *391*, 123622.
[30] Y. H. Song, S. H. Choi, J. S. Yoo, B. K. Kang, E. K. Ji, H. S. Jung, D. H. Yoon, *Chem. Eng. J.* **2017**, *313*, 461.
[31] Z. Shi, J. Guo, Y. Chen, Q. Li, Y. Pan, H. Zhang, Y. Xia, W. Huang, *Adv. Mater.* **2017**, *29*, 1605005.
[32] J. Ren, X. Zhou, Y. Wang, *Nano Res.* **2020**, *13*, 3387.
[33] P. Yang, G. Liu, B. Liu, X. Liu, Y. Lou, J. Chen, Y. Zhao, *Chem. Commun.* **2018**, *54*, 11638.
[34] F. Angel-Huerta, M. P. González-Araoz, J. S. Arias-Cerón, J. F. Sánchez-Ramírez, J. Díaz-Reyes, J. L. Herrera-Pérez, J. G. Mendoza-Álvarez, *J. Mater. Sci.: Mater. Electron.* **2018**, *29*, 15649.
[35] J. L. Stein, E. A. Mader, B. M. Cossairt, *J. Phys. Chem. Lett.* **2016**, *7*, 1315.
[36] A. Buffard, S. Dreyfuss, B. Nadal, H. Heuclin, X. Xu, G. Patriarche, N. Mézailles, B. Dubertret, *Chem. Mater.* **2016**, *28*, 5925.
[37] H. C. Wang, H. Zhang, H. Y. Chen, H. C. Yeh, M. R. Tseng, R. J. Chung, S. Chen, R. S. Liu, *Small* **2017**, *13*, 1603962.
[38] H. Li, Y. Bian, W. Zhang, Z. Wu, T. K. Ahn, H. Shen, Z. Du, *Adv. Funct. Mater.* **2022**, *32*, 2204529.
[39] H. Li, W. Zhang, Y. Bian, T. K. Ahn, H. Shen, B. Ji, *Nano Lett.* **2022**, *22*, 4067.
[40] D. Hahm, J. H. Chang, B. G. Jeong, P. Park, J. Kim, S. Lee, J. Choi, W. D. Kim, S. Rhee, J. Lim, D. C. Lee, C. Lee, K. Char, W. K. Bae, *Chem. Mater.* **2019**, *31*, 3476.
[41] D. A. Granada-Ramirez, J. S. Arias-Ceron, M. Perez-Gonzalez, J. P. Luna-Arias, A. Cruz-Orea, P. Rodriguez-Fragoso, J. L. Herrera-Perez, M. L. Gomez-Herrera, S. A. Tomas,

F. Vazquez-Hernandez, A. A. Duran-Ledezma, J. G. Mendoza-Alvarez, *Appl. Surf. Sci.* **2020**, *530*, 147294.
[42] Y. H. Won, O. Cho, T. Kim, D. Y. Chung, T. Kim, H. Chung, H. Jang, J. Lee, D. Kim, E. Jang, *Nature* **2019**, *575*, 634.
[43] D. A. Taylor, J. A. Teku, S. Cho, W.-S. Chae, S.-J. Jeong, J.-S. Lee, *Chem. Mater.* **2021**, *33*, 4399.
[44] Y. Kim, S. Ham, H. Jang, J. H. Min, H. Chung, J. Lee, D. Kim, E. Jang, *ACS Appl. Nano Mater.* **2019**, *2*, 1496.
[45] W.-S. Song, H.-S. Lee, J. C. Lee, D. S. Jang, Y. Choi, M. Choi, H. Yang, *J. Nanopart. Res.* **2013**, *15*, 1750.
[46] J.-H. Jo, D.-Y. Jo, S.-H. Lee, S.-Y. Yoon, H.-B. Lim, B.-J. Lee, Y. R. Do, H. Yang, *ACS Appl. Nano Mater.* **2020**, *3*, 1972.
[47] J.-H. Jo, D.-Y. Jo, S.-W. Choi, S.-H. Lee, H.-M. Kim, S.-Y. Yoon, Y. Kim, J.-N. Han, H. Yang, *Adv. Opt. Mater.* **2021**, *9*, 2100427.
[48] M. D. Tessier, D. Dupont, K. De Nolf, J. De Roo, Z. Hens, *Chem. Mater.* **2015**, *27*, 4893.
[49] W. Shen, H. Tang, X. Yang, Z. Cao, T. Cheng, X. Wang, Z. Tan, J. You, Z. Deng, *J. Mater. Chem. C* **2017**, *5*, 8243.
[50] G. Laufersky, S. Bradley, E. Frecaut, M. Lein, T. Nann, *Nanoscale* **2018**, *10*, 8752.
[51] J. Zhang, H. Gu, *Dalton Trans.* **2020**, *49*, 6119.
[52] W. Zhang, S. Ding, W. Zhuang, D. Wu, P. Liu, X. Qu, H. Liu, H. Yang, Z. Wu, K. Wang, X. W. Sun, *Adv. Funct. Mater.* **2020**, *30*, 2005303.
[53] H. Zhang, X. Ma, Q. Lin, Z. Zeng, H. Wang, L. S. Li, H. Shen, Y. Jia, Z. Du, *J. Phys. Chem. Lett.* **2020**, *11*, 960.
[54] J. Joo, Y. Choi, Y.-H. Suh, C.-L. Lee, J. Bae, J. Park, *J. Ind. Eng. Chem.* **2020**, *88*, 106.
[55] K.-H. Kim, J.-H. Jo, D.-Y. Jo, C.-Y. Han, S.-Y. Yoon, Y. Kim, Y.-H. Kim, Y. H. Ko, S. W. Kim, C. Lee, H. Yang, *Chem. Mater.* **2020**, *32*, 3537.
[56] Y. Kim, K. Yang, S. Lee, *J. Mater. Chem. C* **2020**, *8*, 7679.
[57] P. Ramasamy, N. Kim, Y.-S. Kang, O. Ramirez, J.-S. Lee, *Chem. Mater.* **2017**, *29*, 6893.
[58] R. P. Brown, M. J. Gallagher, D. H. Fairbrother, Z. Rosenzweig, *Langmuir* **2018**, *34*, 13924.
[59] K. Kim, D. Yoo, H. Choi, S. Tamang, J. H. Ko, S. Kim, Y. H. Kim, S. Jeong, *Angew. Chem., Int. Ed. Engl.* **2016**, *55*, 3714.
[60] F. Pietra, L. De Trizio, A. W. Hoekstra, N. Renaud, M. Prato, F. C. Grozema, P. J. Baesjou, R. Koole, L. Manna, A. J. Houtepen, *ACS Nano* **2016**, *10*, 4754.
[61] Y. Hinuma, A. Grüneis, G. Kresse, F. Oba, *Phys. Rev. B* **2014**, *90*, 155405.
[62] P. Ramasamy, B. Kim, M. S. Lee, J. S. Lee, *Nanoscale* **2016**, *8*, 17159.
[63] A. Vikram, A. Zahid, S. S. Bhargava, L. P. Keating, A. Sutrisno, A. Khare, P. Trefonas, M. Shim, P. J. A. Kenis, *Chem. Mater.* **2020**, *32*, 3577.